Innovative tools for offshore wind and DC grids

Deliverable 1.4 – Work Package 1
Toolboxes of a general modelling method for power electronic converters, MMC control design and designing and analysing DC transformers.

Dissemination level	Other
Website	http://innodc.org/
Grant Agreement number	765585
Due delivery	Month 30: 29 February 2020
Project dates	01/09/2017 – 31/08/2021

Authors	**Names**
ESR1	Peng Yang
ESR4	Davide Pinzan
ESR5	Daniel Westerman Spier
ESR12	Stephen Hardy
ESR14	Motaz Ayiad
Supervisor (KU Leuven)	Hakan Ergun
Supervisor (UPC) WP1 leader	Eduardo Prieto-Araujo

Summary

This document contains a description of the InnoDC project Deliverable 1.4. It develops toolboxes to model SiC MOSFETs for power electronics converters and to model and calculate the optimal current references of the modular multilevel converter under normal and constraint scenarios.

Contents

1 Introduction

1.1 Modular Multilevel Converter

Modular multilevel converters have become the preferred choice for modern High Voltage DC (HVDC) transmission systems [1, 2, 3]. Compared to classic two-level Voltage Source Converters (VSC), MMCs present easier scalability to higher voltages, improved efficiency due to lower switching frequencies and higher output voltage quality [4, 5, 6]. MMCs also have additional degrees of freedom that can be used for an improved converter performance [7], specially during AC and DC network imbalances.

The three-phase MMC (see Fig. 1) is a VSC consisting of three legs, one per phase, in which each leg has two stacks of N_{arm} sub-modules, known as the upper and lower arms. The sub-modules can vary from simple topologies such as the half-bridge or full-bridge to complex ones, based on the application requirements [8]. The main quantities for each phase, considering $k \in (a, b, c)$, are the AC grid voltages u_g^k, the upper and lower arms voltages u_u^k and u_l^k, the upper and lower DC grid voltages U_u^{DC} and U_l^{DC}, the upper and lower arm currents i_u^k and i_l^k and the AC grid current i_s^k. R_a and L_a are the arm equivalent resistance and inductance and finally, R_s and L_s are the phase reactor equivalent resistance and inductance.

In order to adequately exploit the converter's degrees of freedom, the important complexity of the MMC requires models to provide full comprehension of its working principles and the distinct roles of its inner quantities. Relevant previous works on the MMC analysis have been done for both normal and fault scenarios. For normal operation, distinct studies have been performed to analyze the MMC steady-state and dynamic behavior to design the passive elements of the converter [9, 10, 11]. For unbalanced AC faults, different analysis have also been developed. In [12], the steady-state model of the MMC is derived in the synchronous $dq0$ frame considering positive and negative sequence components, focusing on the AC side quantities. An alternative analysis method is to derive the steady-state equations in the *abc* additive x^{Σ} and differential x^{Δ} frame [13, 14, 15, 16], which gives additional appreciation on the converter analysis. In [13], a model of the MMC in the *abc* frame is proposed for unbalanced grid conditions in order to suppress the injection of AC current components into the DC side of the converter. However, the characteristics of the AC network during the fault are based only on the positive sequence. To provide insights about the interactions between the positive and negative sequence components of the AC grid, [14] and [15] used both components during the model derivation. Also, in [16], an optimization algorithm based on Lagrange multipliers is proposed

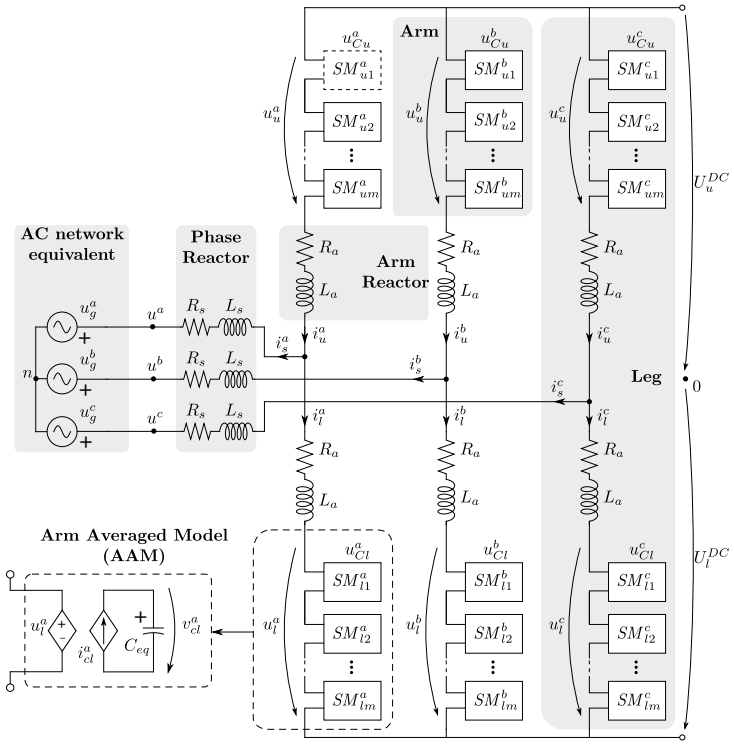

Figure 1: Complete model of the MMC converter.

to calculate the MMC circulating current considering the positive, negative and zero sequence components of the AC side of the converter.

The aforementioned models, although accurately represent the MMC converter, might not be straightforwardly usable in an optimization environment where constraints in the natural *abc* frame should be imposed to individual arm quantities. A natural *abc* per arm modelling approach provides a direct identification of the quantities of the converter. Based on this approach, references [17, 18] proposed a steady-state analysis of the MMC focusing on the AC arm quantities, while considering per phase model of the DC ones, without analyzing DC unbalances.

In terms of converter operation, during unbalanced faults the MMC control should be able to prioritize the AC current components (active or reactive) to be injected into the network to meet the requirements imposed by the grid codes. For instance, reference [19] prioritizes the active current components, whereas [20, 21] main concern is the injection of reactive current to provide voltage support during the fault. In addition, these conditions should be met without violating any of the voltage and current limitations of the converter.

Therefore, an optimization algorithm to calculate the converter references, using a complete per arm MMC model running on the natural *abc* reference frame, able to meet the grid operator specifications while considering the constraints of the MMC (arm currents, voltages and sub-module voltages) for any grid AC and DC voltage condition is formulated. Next, the characteristics of the optimal methodology are:

- Development of a natural *abc* reference frame steady-state model including all the MMC degrees of freedom.
- Formulation of an optimization-based reference calculation problem using the steady-state developed model, to guarantee an optimal MMC operation under any network voltage conditions and grid operator requirements, considering the converter limitations.

The suggested reference calculation optimization problem ensures that:

- The AC currents are as close as possible to the grid code requirements, without exceeding the MMC limits.
- The internal currents of the converter are limited per arm simultaneously considering both AC and DC components.
- Converter applied voltages do not exceed the limitations of the MMC arms.
- Sub-modules voltages do not exceed their voltage limitation. This constraint is imposed using an equivalent arm capacitor modelling which includes the corresponding voltage fluctuation (assuming that an adequate sorting algorithm is implemented).
- The degrees of freedom of the MMC are fully exploited by the optimization to be as close as possible to the operator requirements.
- Any AC grid operator requirement can be fulfilled, prioritizing either active or reactive current component. In this paper, the reactive AC current is prioritized in order to provide voltage support to the faulted network.
- It can be used for different MMC sub-module configurations (half-bridge, full-bridge, hybrid), as long as the MMC limits are adapted according to each equivalent arm voltage condition.

1.2 DC transformer switches modelling

Semiconductor switches are the key component to build power electronic converters such as MMC and DC transformers. Si IGBTs have been widely used in various applications. Comparing to Si IGBTs, Silicon carbide (SiC) MOSFETs have the advantages such as low on-resistance, fast switching speed and high junction temperature capability [22], which allows the power electronics converters to achieve higher power density. However, high speed operation of SiC devices brings to more serious eletromagnetic interface (EMI) issues due to the higher dv/dt and di/dt during the switching transient [23]. Moreover, the efficiency and power density of the converters highly depend on the switching losses during the switching transient. Therefore, an accurate model for SiC MOSFETs is needed to simulate the switching transient [24]. Different models have been presented in the literature [23, 24, 25]. However, the parameter extraction of these models are either too complicated or not well-established. Therefore, a spice model of SiC half-bridge modules and its step-by-step modelling method are given. The drain-to-source current, anti-parallel Schottky diode and parasitic capacitance are accurately modelled. The temperature dependency is considered. The step-by-step parameter extraction method based on datasheet is introduced. This modelling method can be easily adopted to different SiC MOSFETs or power modules.

2 Spice model and parameter extraction method of SiC MOSFET half bridge module

2.1 Spice model of SiC MOSFET half bridge module

The model is built based on the datasheet of 1200-V 120-A SiC half-bridge power module CAS120M12BM2 from Wolfspeed. As shown in Fig. 2, the half-bridge module consists of SiC MOSFETs and anti-parallel SiC Schottky diodes. Fig. 2c shows the subcircuit model of the SiC MOSFET with the anti-parallel diode. It can be seen from Fig. 2c that the model consists of three major parts: drain-to-source current model, diode model and capacitor models. The three parts are modelled respectively.

2.2 Drain-to-source current

In Fig. 2c, a voltage-controlled current source I_{DS} and a series resistor R_{D1} are used to model the drain-to-source current of the SiC MOSFET. The model is based on the standard MOSFET level 1 SPICE model [26]:

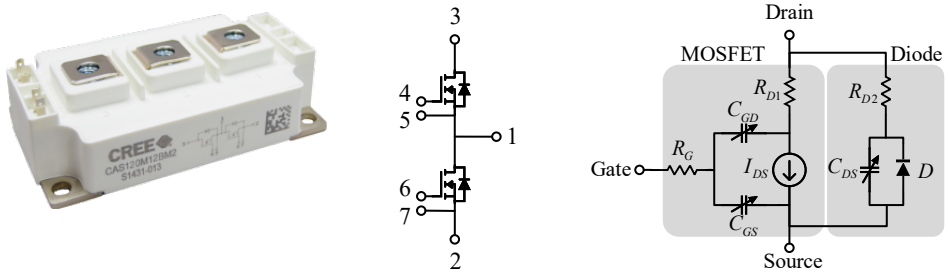

(a) (b) (c)

Figure 2: Package, schematic and equivalent circuit of 1200-V SiC Half-Bridge Module CAS120M12BM2: (a) Package, (b) Schematic, and (c) Sub-circuit model of the SiC MOSFET with the anti-parallel diode in the module.

$$I_{DS} = 0, \quad \text{if } V_{DS} < 0 \text{ or } V_{GS} < V_{GS,th} \tag{1}$$

$$I_{DS} = \beta \left(V_{GS} - V_{GS,th} - \frac{V_{ch}}{2} \right) V_{ch} \left(1 + \lambda V_{ch} \right), \quad \text{if } 0 < V_{DS} < V_{GS} - V_{GS,th} \tag{2}$$

$$I_{DS} = \beta \frac{\left(V_{GS} - V_{GS,th} \right)^2}{2} \left(1 + \lambda V_{ch} \right), \quad \text{if } V_{DS} > V_{GS} - V_{GS,th} \tag{3}$$

$$\beta = \beta_0 + VC \left(V_{GS} - 10 \right) \tag{4}$$

$$V_{ch} = V_{DS} - R_{D1} I_{DS} \tag{5}$$

V_{GS} and V_{DS} are the gate-to-source and the drain-to-source voltages respectively. β_0, VC, $V_{GS,th}$, R_{D1} and λ are the parameters that need to be extracted. The transfer characteristics and output characteristics are used to extract the parameters. The Matlab curve fitting toolbox is used. The parameter extraction procedure is shown in Fig. 3. The extracted parameters are shown in Table 1.

Table 1: Parameters of I_{DS} at 25 °C

β_0	VC	$V_{GS,th}$ (V)	$R_{D1}(\text{m}\Omega)$	λ
4.886	0.2818	3.992	6.001	0.043

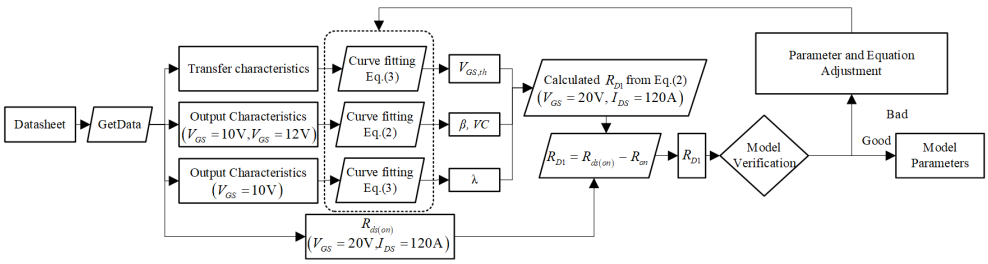

Figure 3: Parameter extraction procedure of I_{DS}.

Table 2: Parameters of diode model

I_S (A)	$R_{D2}(\mathrm{m}\Omega)$
1.925e-14	4.66

To consider the temperature characteristics, the parameters are extracted at different temperatures according to the datasheet. β_0, VC, $V_{GS,th}$ and R_{D1} are modelled as functions of temperature. The temperature dependency of the parameters are shown in Fig. 4. The temperature dependency functions can be obtained as:

$$\begin{cases} \beta_0 = 0.0237T + 4.2227 \\ V_{GS,th} = -0.006T + 4.1416 \\ VC = -0.0039T + 0.3816 \\ R_{D1} = 0.0002T^2 + 0.0214T + 5.3409 \end{cases} \tag{6}$$

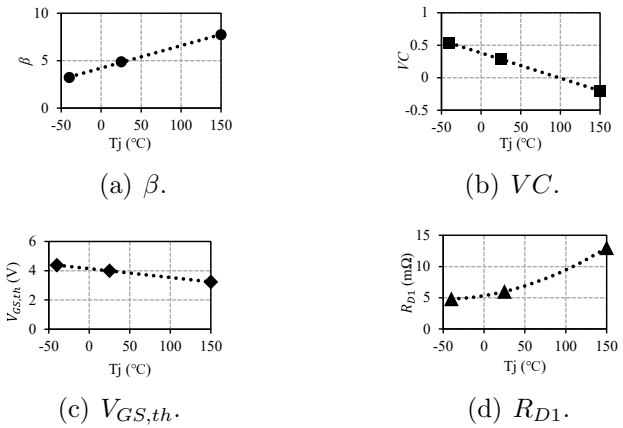

(a) β. (b) VC.

(c) $V_{GS,th}$. (d) R_{D1}.

Figure 4: Temperature dependency of model parameters.

The curve fitting results of output characteristics at different temperatures comparing to datasheet are shown in Fig. 5.

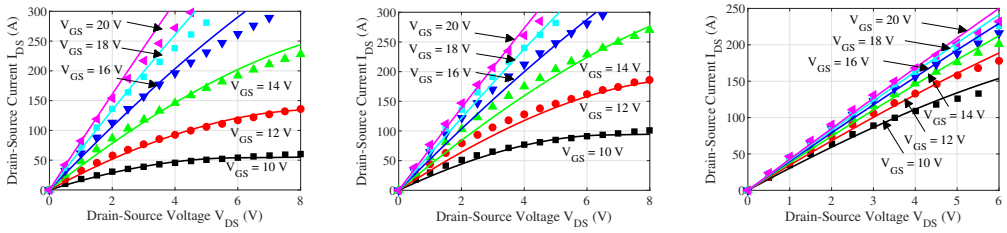

(a) -40 °C. (b) 25 °C. (c) 150 °C.

Figure 5: Output characteristics at different temperatures.

2.3 Anti-parallel Schottky diode

The diode model is shown as follows:

$$I_D = I_S \left(\exp\left(\frac{qV_D}{kT}\right) - 1 \right) \tag{7}$$

$$V_D = V_{SD} - R_{D2} I_D \tag{8}$$

The parameters of the diode model are extracted based on the diode characteristics in the datasheet according to [24]. The extracted parameters are shown in Table 2. The curve fitting results comparing to datasheet are shown in Fig. 6a.

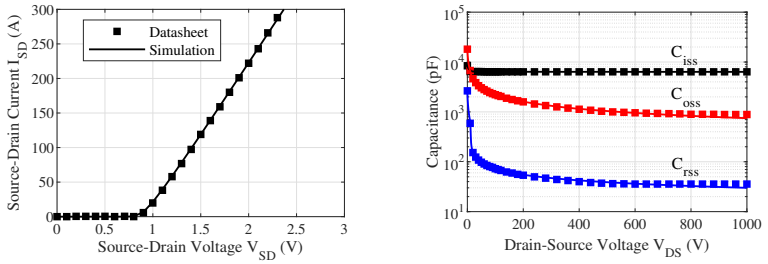

(a) Diode characteristics. (b) Capacitance characteristics.

Figure 6: Characteristics comparison between the model and the datasheet.

2.4 Parasitic capacitance

C_{GS}, C_{GD} and C_{DS} can be calculated by C_{iss},C_{oss} and C_{rss} from the datasheet according to (9). C_{GS} is modelled as a constant capacitor. C_{DS} and C_{GD} are modelled as variable capacitors as shown in (10) [24] and (11) [27]. The model parameters are extracted using Matlab curve fitting toolbox and the results are shown in Table (3). The equation of C_{GD} is very complicated and the parameters need to be extracted step by step. The curve fitting results comparing to datasheet are shown in Fig. 6b.

Table 3: Parameters of capacitance model

C_{GS}(pF)	C_{DS0}(pF)	V_{bi} (V)	M_{CDS}	C_{GD0}(pF)	V_T(V)	k_1	k_2	M_{CGD}
6319	15500	1.622	0.478	2646	13.52	40.51	0.3815	0.4295

$$C_{GD} = C_{rss},\ C_{GS} = C_{iss} - C_{rss},\ C_{DS} = C_{oss} - C_{rss} \tag{9}$$

$$C_{DS} = C_{DS0}\left(\frac{V_{bi}}{V_{DS} + V_{bi}}\right)^{M_{CDS}} \tag{10}$$

$$C_{GD} = \frac{C_{GD0}}{\left(1 + V_{DG}\left(1 + k_1 \frac{1+\tanh\left(k_2(V_{DG}-V_T)\right)}{2}\right)\right)^{M_{CGD}}} \tag{11}$$

2.5 Toolbox to model SiC MOSFETs

Based on the aforementioned model and parameter extraction method, the model parameters, equations, required data inputs and modelling steps can be summarised as:

- 25 model parameters:
  - 5 parameters for drain-to-source current model: $\beta_0, VC, V_{GS,th}, R_{D1}, \lambda$
  - 9 parameters for temperature characteristics
  - 2 parameters for diode model
  - 9 parameters for parasitic capacitance model
- 16 equations divided in:
  - 5 equations for Drain-to-source current model: (1), (2), (3), (4), (5)

- 4 equations for temperature characteristics: (6)
- 2 equations for diode model: (7), (8)
- 5 equations for parasitic capacitance: (9), (10),(11)

The SiC MOSFET model will require the following data inputs to extract the parameters:

- transfer characteristics under different temperature
- output characteristics under different temperature
- $R_{ds(on)}$
- diode characteristics
- capacitance characteristics

The curve fitting toolbox is used to extract the parameters of the model using the data from datasheet. The procedure of parameter extraction is described as:

1. Curve fitting of transfer characteristics and output characteristics to obtain the drain-to-source current model under different temperatures.
2. Curve fitting of temperature parameters to obtain the temperature characteristics.
3. Curve fitting of the diode characteristics to obtain the diode model.
4. Curve fitting of the capacitance characteristics to obtain the parasitic capacitance model.

This modelling procedure can be adopted as a toolbox in order to obtain a model for various SiC MOSFETs and power modules. The model can be further used for simulation, analysis and design of power electronics converters such as DC/DC converters.

3 Steady-state modelling and analysis of the MMC

In this section, the steady-state equations of the MMC are derived considering that it is connected to generic AC and DC networks, which can be either in balanced or unbalanced conditions. The MMC arm quantities contain both AC and DC components. Applying the superposition principle [28], the DC and AC systems can be decoupled and studied separately.

3.1 AC network currents

For steady-state analysis purposes, the phasorial notation $\underline{X}^k = X_r^k + jX_i^k = X^k \angle \underline{\theta^k}$ will be adopted, with $x(t) = X^k \Re(e^{j(\omega t + \theta^k)})$ and $k \in (a, b, c)$. The model assumes that the per phase active I_P^k and reactive I_Q^k currents set-points are values imposed by the grid operator. Based on the per phase active and reactive currents, the grid currents can be calculated as

$$\begin{bmatrix} I_{s_r}^k \\ I_{s_i}^k \end{bmatrix} = \begin{bmatrix} \cos(\theta^k) & -\sin(\theta^k) \\ \sin(\theta^k) & \cos(\theta^k) \end{bmatrix} \cdot \begin{bmatrix} I_P^k \\ I_Q^k \end{bmatrix} \tag{12a}$$

$$\underline{I}_s^k = I_{s_r}^k + jI_{s_i}^k \tag{12b}$$

where $I_{s_r}^k$ and $I_{s_i}^k$ are the real and imaginary parts of the per-phase AC grid currents. Whereas, θ^k are the phase-angles of the AC grid voltages.

3.2 AC MMC circuit analysis

Fig. 7 shows the AC circuit which can be derived from Fig. 1, short-circuiting the DC voltage sources and considering the AC component of the arm applied voltages.

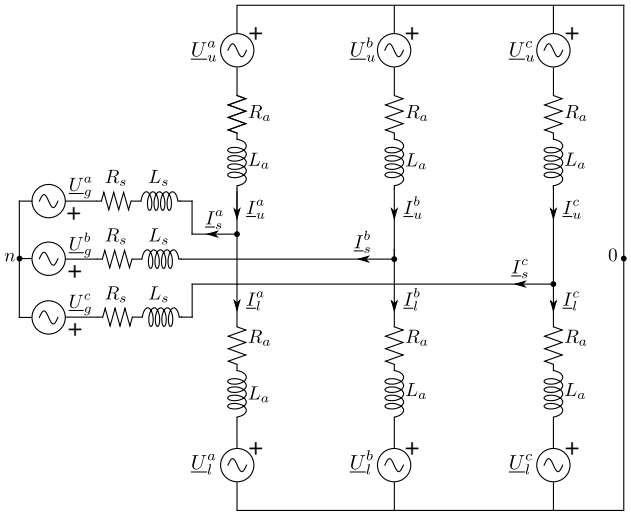

Figure 7: AC model of the MMC.

Applying the Kirchhoff Current Law (KCL) in the middle point of the MMC arms and involving the currents calculated in (12), the relation between the arm currents is obtained as

$$\underline{I}_s^k = \underline{I}_u^k - \underline{I}_l^k \tag{13}$$

To prevent the circulation of AC current through the DC network, no AC zero sequence arms' current component must be flowing through the MMC. This restriction can be met by imposing that the sum of the upper arms' AC currents is equal to zero, as

$$\underline{I}_u^a + \underline{I}_u^b + \underline{I}_u^c = 0 \tag{14}$$

Note that, no additional equation is required to eliminate the zero sequence current component from the lower arms, as it can be directly obtained by combining (13), (14) while assuming no zero sequence in the grid currents (three-wire connection).

The AC voltage equations for the MMC arms (see Fig. 2) can be obtained through Kirchhoff Voltage Law (KVL) assuming that the per phase voltages $\underline{U}_g^k$ are given quantities, as

$$\underline{U}_{0n} = \underline{U}_g^k + \underline{Z}_s(\underline{I}_u^k - \underline{I}_l^k) + \underline{Z}_a\underline{I}_u^k + \underline{U}_u^k \tag{15}$$

$$\underline{U}_{0n} = \underline{U}_g^k + \underline{Z}_s(\underline{I}_u^k - \underline{I}_l^k) - \underline{Z}_a\underline{I}_l^k - \underline{U}_l^k \tag{16}$$

where, $\underline{U}_{0n}$ is the voltage between the 0 DC reference node and the neutral n of the AC three-phase system.

The last equation to be included in the AC analysis is the power difference between the arms, which is required to conduct a first steady-state analysis. In this case, it can be assumed that the upper and lower arms exchange the same amount of active and reactive power, as

$$P_u^k - P_l^k = 0 \rightarrow U_{u_r}^k I_{u_r}^k + U_{u_i}^k I_{u_i}^k = U_{l_r}^k I_{l_r}^k + U_{l_i}^k I_{l_i}^k \tag{17}$$

$$Q_u^k - Q_l^k = 0 \rightarrow U_{u_r}^k I_{u_i}^k - U_{u_i}^k I_{u_r}^k = U_{l_r}^k I_{l_i}^k - U_{l_i}^k I_{l_r}^k \tag{18}$$

Later, (17) and (18) will not be part of the optimization, as they will be considered a degree of freedom of the converter, as discussed in Section 5.

3.3 DC MMC circuit analysis

For the DC part of the MMC, an analogous analysis to the AC circuit is developed. The DC model is shown in Fig. 8, where only DC voltages are applied to the system, short-circuiting the AC sources and inductances.

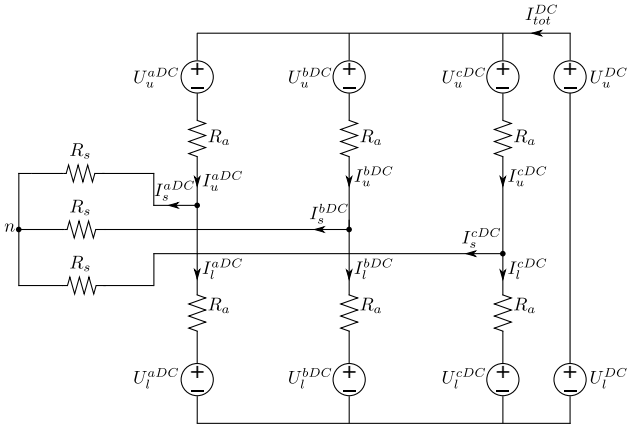

Figure 8: DC model of the MMC.

In order to avoid the circulation of DC components into the AC network, I_s^{kDC} is regulated to be equal to zero. Therefore, $I_u^{kDC} = I_l^{kDC} = I^{kDC}$, with $k \in (a, b, c)$. The voltage equations can be written as follows

$$U_u^{DC} + U_l^{DC} = U_u^{kDC} + U_l^{kDC} + 2R_a I^{kDC} \tag{19}$$

Also, the total DC current of the system I_{tot}^{DC} can be obtained as

$$I_{tot}^{DC} = I^{aDC} + I^{bDC} + I^{cDC} \tag{20}$$

3.4 Steady-state AC/DC power balance equations

In steady-state conditions, the AC and DC active power exchanged in each of the arms (voltage sources) should be equal, if the semi-conductor losses are neglected. Obviously, this is not feasible with instantaneous values (as the arm single-phase AC power is non-constant). However, it is possible to impose an equality between the AC average power (calculated in the phasor domain) and the DC power. If this condition is not achieved, the energy in the arm cells would either charge or discharge the equivalent arm capacitors (increasing/decreasing the stored energy) and therefore, steady-state conditions would not hold. This constraint can be mathematically expressed

$$P_{u,l}^{kAC} = P_{u,l}^{kDC} \rightarrow U_{u,l_r}^{k} I_{u,l_r}^{k} + U_{u,l_i}^{k} I_{u,l_i}^{k} = U_{u,l}^{kDC} I^{kDC} \tag{21}$$

3.5 Equivalent arm capacitor voltage fluctuation

Next, an estimation of the equivalent arm capacitor (see Fig. 1) voltage ripple is performed in order to verify that the sub-module capacitor voltages do

not exceed their design limitations. The energy stored in each arm of the converter is directly dependant on the power flowing through the MMC. Under balanced AC network conditions, the average energy stored in each arm is equal, also showing similar ripple profiles per arm (phase-shift difference). However, during unbalanced scenarios, the MMC arms may present high energy deviations, leading to variations of the energy stored within them, which might eventually exceed the design limitations. Consequently, the energy stored in each arm, therefore in each submodule (assuming an adequate sorting algorithm), must be kept within a certain range to ensure a proper operation of the MMC.

To mathematically represent the equivalent arm voltage fluctuation, the Arm Averaged Model (AAM) [29] is used (see Fig. 1). This model represents each arm as an equivalent capacitor that is charged/discharged depending on the power exchanged by each arm, which is reflected as a charging/discharging current. This way, the entire arm can be represented as an equivalent capacitor. Based on the AAM equivalent arm model, a mathematical procedure to derive a generalized estimation for the maximum and minimum voltage ripple for the equivalent arm capacitor is presented.

3.5.1 Instantaneous MMC arm power

To calculate the equivalent arm capacitor voltage ripple, firstly, the instantaneous power for the upper and lower arms of the MMC should be obtained as

$$p_{u,l}^{k}(t) = u_{u,l}^{k}(t) i_{u,l}^{k}(t) = \left(U_{u,l}^{kDC} + \hat{U}_{u,l}^{k}\cos(\omega t + \psi_{u,l}^{k})\right) \left(I_{u,l}^{kDC} + \hat{I}_{u,l}^{k}\cos(\omega t + \delta_{u}^{k})\right) \tag{22}$$

where $I_{u,l}^{kDC}$ are the upper and lower DC currents flowing through the MMC arms, $\delta_{u,l}^{k}$ and $\psi_{u,l}^{k}$ are the upper and lower arms' currents and voltages phase-angles, respectively. It can be noted that the power will have components at zero, ω and 2ω pulsations. The sum of the constant zero frequency power of the AC and DC sources must be zero in steady-state conditions, to avoid energy deviation in the arm. Therefore, the upper and lower arms' powers [30] can be reduced to

$$p_{u,l}^{k}(t) = U_{u,l}^{kDC}\hat{I}_{u,l}^{k}\cos(\omega t + \delta_{u,l}^{k}) + \tag{23}$$
$$+ I_{u,l}^{kDC}\hat{U}_{u,l}^{k}\cos(\omega t + \psi_{u,l}^{k}) + \frac{\hat{U}_{u,l}^{k}\hat{I}_{u,l}^{k}}{2}\cos(2\omega t + \delta_{u,l}^{k} + \psi_{u,l}^{k})$$

3.5.2 Arms maximum energy and voltage calculation

The capacitor voltage presents a profile that is related to its energy. One way to find the maximum and minimum values of the equivalent arm capacitor voltage is to obtain the peak values of the arm energy. The equation for the instantaneous energy flowing through the MMC arms can be expressed as (integrating (23) over time)

$$E^k_{u,l}(t) = \frac{U^{kDC}_{u,l}\hat{I}^k_{u,l}}{\omega}\sin(\omega t + \delta^k_{u,l}) + \\ + \frac{I^{kDC}_{u,l}\hat{U}^k_{u,l}}{\omega}\sin(\omega t + \psi^k_{u,l}) + \frac{\hat{U}^k_{u,l}\hat{I}^k_{u,l}}{4\omega}\sin(2\omega t + \delta^k_{u,l} + \psi^k_{u,l}) \tag{24}$$

Based on the analysis conducted in [30], the maximum energy fluctuation for the MMC upper and lower arms $E^{kAC}_{u,l_{max}}$ can be obtained as given in (25).

$$E^{kAC}_{u,lmax} \approx \sqrt{\left[\frac{U^{kDC}_{u,l}\hat{I}^k_{u,l}}{\omega}\cos(\delta^k_{u,l}) + \frac{I^{kDC}_{u,l}\hat{U}^k_{u,l}}{\omega}\cos(\psi^k_{u,l})\right]^2 + \left[\frac{U^{kDC}_{u,l}\hat{I}^k_{u,l}}{\omega}\sin(\delta^k_{u,l}) + \frac{I^{kDC}_{u,l}\hat{U}^k_{l}}{\omega}\sin(\psi^k_{u,l})\right]^2} + \left|\frac{\hat{U}^k_{u,l}\hat{I}^k_{u,l}}{4\omega}\right| \tag{25}$$

Considering steady-state conditions, the MMC equivalent arms' capacitors are storing the nominal DC energy, obtained as

$$E^k_{u,l_{ref}} = \frac{C_{SM}}{2}N^k_{u,l_{arm}}U^2_{SM} \tag{26}$$

where U_{SM} is average sub-module nominal voltage, C_{SM} is the sub-module capacitance and $N^k_{u,l_{arm}}$ is the number of sub-modules available in the arm. Therefore, the maximum and minimum values for the upper and lower arms energy can be obtained adding (25) and (26), described as

$$E^k_{u,l_{max,min}} = \underbrace{E^k_{u,l_{ref}}}_{\text{DC term (26)}} \pm \underbrace{E^{kAC}_{u,l_{max}}}_{\text{peak of the AC part (25)}} \tag{27}$$

Based on the maximum and minimum energy levels $E^k_{u,l_{max,min}}$, the admissible voltage magnitudes of the equivalent arms' capacitors can be expressed as

$$U^k_{Cu,l_{max,min}} = \sqrt{\frac{2E^k_{u,l_{max,min}}N^k_{u,l_{arm}}}{C_{SM}}} \tag{28}$$

3.5.3 Complete model

The full non-linear steady-state model for the MMC, with $k \in (a, b, c)$, can be summarized as,

- 72 quantities given as:
  - 13 complex AC quantities: $\underline{U}^k_{u,l}$, $\underline{U}_{0n}$, $\underline{I}^k_{u,l}$
  - 46 DC quantities: $U^{kDC}_{u,l}, I^{kDC}, I^{DC}_{tot}$, $E^{kAC}_{u,l_{max}}$, $E^k_{u,l_{ref}}$ $E^k_{u,l_{max,min}}$, $U^k_{Cu,l_{max,min}}$
- 72 equations divided as:
  - 10 complex linear AC equations: (13) to (16)
  - 4 linear DC real equations: (19), (20)
  - 48 non-linear real equations: (17), (18), (21), (25-28)

The model will require the following inputs

- AC and DC system voltages: $\underline{U}^k_g$, $U^{DC}_{u,l}$.
- AC network current $\underline{I}^k_s$ obtained using (12), based on I^k_P and I^k_Q.
- Sub-module characteristics: U_{SM}, C_{SM}, $N^k_{u,l_{arm}}$.

This model can be employed to calculate the steady-state quantities of the MMC for any grid voltage condition. In addition, it will be adapted in Section 5 to be used as an optimization-based toolbox reference calculation. It will also be utilized to calculate the pre-faults values of the system, to be added as initial conditions for the optimization algorithm to increase the speed of conversion.

4 Grid support requirements

This section details the calculation of the AC side currents dictated by the operators' grid codes. During an AC grid voltage fault, the MMC must be able to inject or absorb reactive or active currents from the AC grid in order to provide voltage or frequency support, respectively. According to the Spanish grid code [21] (taken as example), the HVDC system must prioritize voltage support. Therefore, the magnitude of the reactive current to be injected ΔI_r(in pu basis) into the grid, in an AC grid voltage sag occurance, varies according to AC system RMS voltage levels as follows

1. $U_{min1} \leqslant U^k_g \leqslant U_{max1} \rightarrow \Delta I^k_r = 0$
2. $U_{min2} \leqslant U^k_g < U_{min1} \rightarrow \Delta I^k_r = \dfrac{\Delta I_{rmax}(U_{min1} - U^k_g)}{U_{min1} - U_{min2}}$

3. $U_g^k < U_{min2} \rightarrow \Delta I_r^k = \Delta I_{rmax}$

Under a balanced fault, the injection of reactive currents presents a symmetrical profile. However, in an unbalanced AC voltage sag condition, the three-phase system may have different voltage levels in each of its phases [31].

Previous versions of the grid code imposed that the voltage support must be based only on the positive sequence component of the faulted AC grid voltage. However, this methodology is unable to provide full voltage support to the faulted grid. By disregarding the others voltage sequence components, healthy phases might receive unnecessary voltage support leading to overvoltages in the system. The opposite scenario may also happen, where the faulted phases might require full voltage support but, the value of the reactive current calculated based only on the positive sequence voltage component is insufficient.

On the other hand, by considering all the three symmetrical (positive, negative and zero) AC voltages components, the phases would receive the exact amount of reactive and active power in accordance to the grid code. Nonetheless, such a strategy may be infeasible since the AC system consists of three-wires and this strategy might try to impose a zero sequence current component into the AC network.

Therefore, an optimization strategy is suggested to adjust each individual phase current to be as close as possible to the grid code (active and specially reactive) power support requests, without violating the converter constraints and limits. Firstly, the pre-fault active and reactive AC grid current components are obtained as

$$\begin{bmatrix} I_{P_{pre}}^k \\ I_{Q_{pre}}^k \end{bmatrix} = \begin{bmatrix} \cos(\theta_{pre}^k) & \sin(\theta_{pre}^k) \\ -\sin(\theta_{pre}^k) & \cos(\theta_{pre}^k) \end{bmatrix} \cdot \begin{bmatrix} I_{spre_r}^k \\ I_{spre_i}^k \end{bmatrix} \tag{29}$$

where θ_{pre}^k and $\underline{I}_{spre}^k$ are the phase-angle of the AC grid voltages and the AC grid currents during pre-fault conditions (obtained using (12)), respectively. The support current to fulfill the grid code requirements is calculated adding the additional required reactive current to the pre-fault reactive current component, as $I_{sup}^k = \Delta I_r^k + I_{Q_{pre}}^k$. This magnitude is expressed as a phasor, which has to be properly placed in relation to the faulted AC grid voltages to allow voltage support, as (considering $k \in (a, b, c)$)

$$\underline{I}_{sup}^k = I_{sup}^k(\cos(\theta_F^k + 90^o) + j\sin(\theta_F^k + 90^o)) \tag{30}$$

where θ_F^k is the phase-angle of the AC grid voltages during the fault. However, if such current is small than the AC grid current limitations I_{max}^{AC},

$|I^k_{sup}| < I^{AC}_{max}$, the grid code demands the MMC to also inject active current components $\underline{I}^k_P$, which must have the same phase-angles as the faulted AC grid voltages, until the AC grid currents achieve nominal levels. This active current component can be described as

$$\underline{I}^k_P = I^k_P(\cos(\theta^k_F) + j\sin(\theta^k_F)) \tag{31}$$

where I^k_P is the magnitude of the AC active current, which is equal to the pre-fault active current component $I^k_{P_{pre}}$. As an example, for a type C fault [31], the voltages and current vectors are depicted in Fig. 9. For an easier understanding of the phasors, a pre-fault state with $I^k_{Q_{pre}} = 0$ has been chosen.

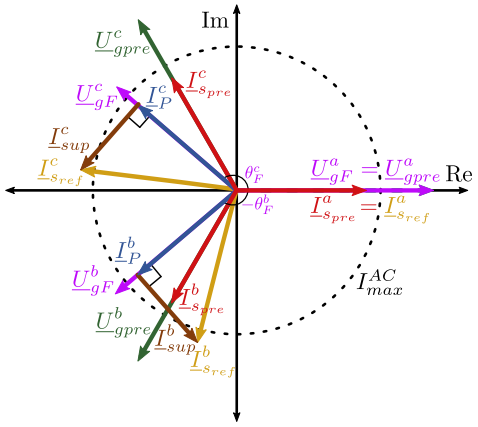

Figure 9: Reactive current injection according to the utility grid voltage.

Although the addition of $I^k_{P_{pre}}$ may result in AC grid currents that are higher than the nominal levels or even exceeding the system limitations, the optimization problem is formulated to avoid those issues. To do so, the active I^k_P and reactive I^k_Q components have to be adjusted to calculate AC grid current references $\underline{I}^k_{s_{ref}}$ that do not exceed the design limitations. This can be achieved by adding to (29) the coefficients (α^k and β^k), which are used to adapt the amount of active and reactive currents to be injected per phase in case of reaching a limitation. Then, $\underline{I}^k_{s_{ref}}$ can be calculated as

$$\begin{bmatrix} I^k_{s_{ref_r}} \\ I^k_{s_{ref_i}} \end{bmatrix} = \begin{bmatrix} \cos(\theta^k_F) & -\sin(\theta^k_F) \\ \sin(\theta^k_F) & \cos(\theta^k_F) \end{bmatrix} \cdot \begin{bmatrix} \alpha^k \cdot I^k_P \\ \beta^k \cdot I^k_Q \end{bmatrix} \tag{32}$$

As mentioned above, the coefficients α^k and β^k can affect the active and reactive currents levels, respectively. Under normal operations, both parameters present their maximum level being equal to 1, which would not

constraint either the active or the reactive powers. However, depending on the AC grid voltage conditions, these values should be modified to remove both the zero sequence current component of the unbalanced references and to meet the MMC limitations. Clearly, the selection of the six coefficients α^k and β^k is not a simple task as changing any of the coefficients will importantly affect the response of the converter towards the network. Thus, the reference calculation problem will be part of an optimization problem, which will ensure that the current references are as close as possible in terms of active and reactive powers to the grid code demands (enabling also active/reactive power prioritization). This strategy is named Optimal Strategy and the optimization problem used to calculate it is detailed in the next section.

5 Optimal reference calculation

In this section, an optimization algorithm is proposed to calculate the converter arm quantities in order to provide adequate grid support during balanced and unbalanced voltage conditions while ensuring that the converter operation is kept within its design and operating limits.

5.1 Optimization problem

The multi-objective function is defined in (33), where each term of the expression is multiplied by a weighting factor λ_x that is used to prioritize among converter arm inductance losses λ_1, active power λ_2 and reactive power λ_3. In this paper, $\lambda_3 \gg \lambda_2 \gg \lambda_1$ so that the reactive current is prioritized over the active current and the power losses (pushing β^k as close as possible to 1), respectively.

$$\text{minimize W}\left(\alpha^k, \beta^k, \underline{I}^k_{u,l}, I^{kDC}_{u,l}, I^{DC}_{tot}, \underline{I}^k_{s_{ref}}, \underline{U}^k_{u,l}, U^{kDC}_{u,l}, \underline{U}_{0n}, E^k_{u,l_{ref}} E^{kAC}_{u,l_{max}}, E^k_{u,l_{max,min}}, U^k_{Cu,l_{max,min}}\right) =$$
$$\lambda_1 \left(R_a \left(\sum_{k=a}^{c} I_u^{k\,2} + I_l^{k\,2} \right) + R_a \left(\sum_{k=a}^{c} I_u^{kDC\,2} + I_l^{kDC\,2} \right) \right) - \lambda_2 \left(\sum_{k=a}^{c} \alpha^k \right) - \lambda_3 \left(\sum_{k=a}^{c} \beta^k \right) \tag{33}$$

To ensure that all the technical constraints are fulfilled, the optimization problem is subjected to several linear and non-linear constraints. These mathematical restrictions are based on the equations of the steady-state model presented in Section 3. Specifically, (14), (15) and (16), together with the following linear constraints are part of the optimization problem, considering $k \in (a, b, c)$

$$\underline{I}^{a}_{s_{ref}} + \underline{I}^{b}_{s_{ref}} + \underline{I}^{c}_{s_{ref}} = 0 \tag{34a}$$

$$\underline{I}^{k}_{s_{ref}} = \underline{I}^{k}_{u} - \underline{I}^{k}_{l} \tag{34b}$$

$$U^{DC}_{u,l} = U^{kDC}_{u,l} + R_a I^{kDC}_{u,l} \tag{34c}$$

$$I^{kDC}_{s_{ref}} = I^{kDC}_{u} - I^{kDC}_{l} \tag{34d}$$

$$I^{DC}_{tot} = I^{aDC}_{u} + I^{bDC}_{u} + I^{cDC}_{u} \tag{34e}$$

Equation (34a) imposes that the AC current references have no zero sequence component, while (34b) describes the relation between the MMC AC currents. Equations (34c) and (34d) are included to guarantee that no DC current flows through the AC side of the converter. Finally, (34e) relates the MMC inner DC currents with the total DC one. For the non-linear constraints, (32) is needed along with the AC/DC arm power balance equations

$$P^{kAC}_{u,l} = P^{kDC}_{u,l} \rightarrow U^{k}_{u,l_r} I^{k}_{u,l_r} + U^{k}_{u,l_i} I^{k}_{u,l_i} = U^{kDC}_{u,l} I^{kDC}_{u,l} \tag{35}$$

In addition to the expressions shown above, the energy equations for the upper and lower capacitor arms (25)-(27) are also required, since they are used to calculate the equivalent arms' capacitor voltages. Lastly, the converter limitations are imposed by the following inequalities

$$I^{k}_{s_{ref}} \leqslant I^{AC}_{max}, \quad I^{k}_{u,l} + I^{kDC}_{u,l} \leqslant I^{arm}_{max} \tag{36a}$$

$$U^{k}_{Cu,l_{max}} \leqslant U_{C_{max}} \tag{36b}$$

$$0 \leqslant U^{kDC}_{u,l} + \sqrt{2} U^{k}_{u,l} \leqslant U^{k}_{Cu,l_{min}} \tag{36c}$$

$$0 \leqslant \alpha^k \leqslant 1, \quad 0 \leqslant \beta^k \leqslant 1 \tag{36d}$$

where I^{AC}_{max} is the maximum current that can be injected into the AC grid, I^{arm}_{max} is the maximum current which can circulate through the MMC arms, and $U_{C_{max}}$ is the peak value that the equivalent arms' capacitors voltage can achieve, that can be directly related to each sub-module voltage. Equations (36a) to (36c) are used to assure that the MMC quantities are maintained within the design limitations. If full-bridge sub-modules were considered, the left value of (36c) should be replaced from 0 to $-U^{k}_{Cu,l_{min}}$. Finally, the weights α^k and β^k are limited as shown in (36d). The optimization will try to maximize these weights (max. equal to 1), consequently being as close as possible to the desired current references imposed by the grid code, respecting the system constraints.

5.2 Toolbox to calculate the optimal MMC quantities

Based on the optimization algorithm derived in the previous section, the system inputs, as well as, the MMC quantities, equations and limitations can be summarized as:

- 90 MMC quantities:
  - 16 AC quantities: $\underline{U}^k_{u,l}, \underline{U}_{0n}, \underline{I}^k_{u,l}, \underline{I}^k_{s_{ref}}$
  - 58 DC quantities: $U^{kDC}_{u,l}, I^{kDC}_{u,l}, I^{kDC}_{s_{ref}}, I^{DC}_{tot}, \alpha^k, \beta^k$, $E^{kAC}_{u,l_{max}}, E^k_{u,l_{ref}}, E^k_{u,l_{max,min}}, U^k_{Cu,l_{max,min}}$
- 80 equations divided in:
  - 11 complex linear AC equations: (14), (15), (16), (34a), (34b)
  - 10 linear DC equations: (34c-34e)
  - 48 non-linear equations: (25-28), (32), (35)
- 39 inequalities: (36a-36d)

The optimal model will require the following inputs:

- AC and DC system voltages: $\underline{U}^k_g$, $U^{DC}_{u,l}$.
- AC network current in the form of active I^k_P and reactive I^k_Q currents, which are obtained using the pre-fault AC current and voltage levels, the reactive current required by the grid code I^k_{sup} and the AC grid phase-angles during the fault θ^k_F.
- Sub-module type and characteristics: U_{SM}, C_{SM}, $N^k_{u,l_{arm}}$.

The different steps to run the optimization algorithm are described as:

1. Definition of the pre-fault and fault condition scenarios.
2. Obtention of the pre-fault MMC steady-state quantities.
3. Calculation of the active and reactive current set-points required by the grid code $\underline{I}^k_P$ and $\underline{I}^k_Q$, see (29-31).
4. Define the weighting factors λ_x of the multi-objective function.
5. Introduce the MMC parameters and limitations.
6. Run the optimization algorithm using equations detailed above.

In addition, the six steps presented above can be further exploited and re-arranged as a flowchart, see Fig. 10. This algorithm can be directly employed as a toolbox in order to obtain the optimal AC references of the MMC.

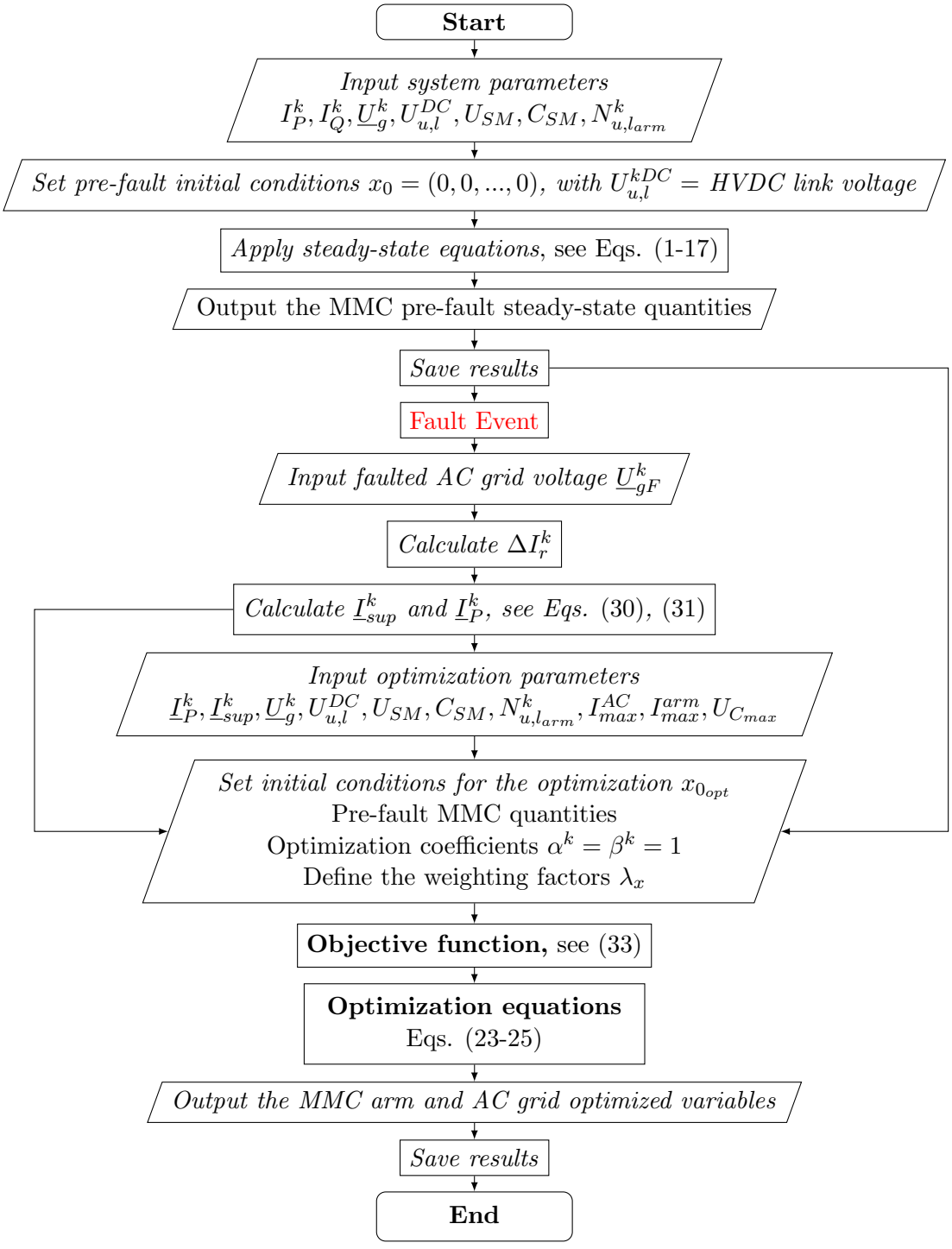

Figure 10: Flowchart of the complete optimization algorithm to provide voltage support.

6 Conclusion

A Spice model of SiC half-bridge power module has been proposed. The Drain-to-source current, anti-parallel Schottky diode and parasitic capacitance are modelled accurately based on the datasheet. The temperature dependency of the model has also been considered. A step-by-step parameter extraction procedure based on the datasheet has been presented, which can be easily adopted to other SiC MOSFETs or power modules. The model can be further used for simulation, analysis and design of power electronics converters such as DC/DC converters, as part of a more complete toolbox.

Furthermore, an optimization-based reference calculation method for MMCs operating in normal and constrained situations (converter variables limited due to voltage or current limitations) has also been presented. The optimization problem has been formulated based on the steady-state per arm approach model, which permits analyzing individually each converter arm while enabling to impose specific arm constraints. The limitations considered have been each individual arm currents and voltages and the sub-module capacitor voltages, in which the last one was obtained through an analytic estimation. In addition, the optimization algorithm has been formulated as a multi-objective problem, allowing to prioritize between active power, reactive power or converter arm losses reduction when the converter is operating in a constrained condition.

References

[1] D. Van Hertem, O. Gomis-Bellmunt, and J. Liang. *HVDC Grids: For Offshore and Supergrid of the Future*. IEEE Press Series on Power Engineering. Wiley, 2016.

[2] E. Prieto-Araujo, A. Junyent-Ferré, G. Clariana-Colet, and O. Gomis-Bellmunt. Control of modular multilevel converters under singular unbalanced voltage conditions with equal positive and negative sequence components. *IEEE Trans. Power Syst.*, 32:2131–2141, May 2017.

[3] E. Sánchez-Sánchez, E. Prieto-Araujo, A. Junyent-Ferré, and O. Gomis-Bellmunt. Analysis of MMC energy-based control structures for VSC-HVDC links. *IEEE Trans. Emerg. Sel. Topics Power Electron.*, 6(3):1065–1076, Sep. 2018.

[4] A. Lesnicar and R. Marquardt. An innovative modular multilevel converter topology suitable for a wide power range. In *2003 IEEE Bologna Power Tech Conf. Proc.*, volume 3, page 6 pp., June 2003.

[5] S. Rohner, S. Bernet, M. Hiller, and R. Sommer. Modulation, losses, and semiconductor requirements of modular multilevel converters. *IEEE Trans. Ind. Electron.*, 57(8):2633–2642, Aug 2010.

[6] J. Peralta, H. Saad, S. Dennetiere, J. Mahseredjian, and S. Nguefeu. Detailed and averaged models for a 401-level MMC-HVDC system. *IEEE Trans. Power Del.*, 27(3):1501–1508, July 2012.

[7] Eduardo Prieto-Araujo, Adriá Junyent-Ferré, Carlos Collados-Rodríguez, Gerard Clariana-Colet, and Oriol Gomis-Bellmunt. Control design of modular multilevel converters in normal and AC fault conditions for HVDC grids. *Electr. Pow. Syst. Res.*, 152:424 – 437, 2017.

[8] Kamran Sharifabadi, Lennart Harnefors, Hans Peter Nee, Staffan Norrga, and Remus Teodorescu. *Design, Control and Application of Modular Multilevel Converters for HVDC Transmission Systems*. Wiley-IEEE press, 2016.

[9] X. Li, Q. Song, W. Liu, S. Xu, Z. Zhu, and X. Li. Performance analysis and optimization of circulating current control for modular multilevel converter. *IEEE Trans. Ind. Electron.*, 63:716–727, Feb 2016.

[10] R. Oliveira and A. Yazdani. An enhanced steady-state model and capacitor sizing method for modular multilevel converters for HVDC applications. *IEEE Trans. Power Electron.*, 33:4756–4771, June 2018.

[11] Ö. C. Sakinci and J. Beerten. Generalized dynamic phasor modeling of the MMC for small-signal stability analysis. *IEEE Trans. Power Del.*, 34(3):991–1000, June 2019.

[12] M. Guan and Z. Xu. Modeling and control of a modular multilevel converter-based HVDC system under unbalanced grid conditions. *IEEE Trans. Power Electron.*, 27(12):4858–4867, Dec 2012.

[13] J. Wang, J. Liang, C. Wang, and X. Dong. Circulating current suppression for MMC-HVDC under unbalanced grid conditions. *IEEE Trans. Ind. Appl.*, 53(4):3250–3259, July 2017.

[14] Y. Liang, J. Liu, T. Zhang, and Q. Yang. Arm current control strategy for MMC-HVDC under unbalanced conditions. *IEEE Trans. Power Del.*, 32(1):125–134, Feb 2017.

[15] Z. Ou, G. Wang, and L. Zhang. Modular multilevel converter control strategy based on arm current control under unbalanced grid condition. *IEEE Trans. Power Electron.*, 33(5):3826–3836, May 2018.

[16] G. Bergna-Diaz, J. A. Suul, E. Berne, J. Vannier, and M. Molinas. Optimal shaping of the MMC circulating currents for preventing AC-side power oscillations from propagating into HVDC grids. *IEEE Trans. Emerg. Sel. Topics Power Electron.*, 7:1015–1030, June 2019.

[17] X. Shi, Z. Wang, B. Liu, Y. Li, L. M. Tolbert, and F. Wang. Steady-state modeling of modular multilevel converter under unbalanced grid conditions. *IEEE Trans. Power Electron.*, 32(9):7306–7324, Sep. 2017.

[18] X. Shi, Z. Wang, B. Liu, Y. Liu, L. M. Tolbert, and F. Wang. Characteristic investigation and control of a modular multilevel converter-based HVDC system under single-line-to-ground fault conditions. *IEEE Trans. on Power Electron.*, 30(1):408–421, Jan 2015.

[19] National Grid TSO. *The Grid Code*, Sept 2019.

[20] Elia. *Proposal for NC HVDC requirements of general application*, May 2018.

[21] Red Elétrica de España. *Procedimiento de Operación 12.4: Requisitos Técnicos Mínimos de Conexión de Sistemas HVDC y Módulos de Parque Eléctrico Conectados en Corriente Continua*, Jun 2018.

[22] Fei Wang, Edward A Jones, and Zheyu Zhang. *Characterization of wide bandgap power semiconductor devices*. Institution of Engineering & Technology, 2018.

[23] H. Sakairi, T. Yanagi, H. Otake, N. Kuroda, and H. Tanigawa. Measurement methodology for accurate modeling of sic mosfet switching behavior over wide voltage and current ranges. *IEEE Trans. Power Electron.*, 33(9):7314–7325, Sep. 2018.

[24] S. Yin, P. Tu, P. Wang, K. J. Tseng, C. Qi, X. Hu, M. Zagrodnik, and R. Simanjorang. An accurate subcircuit model of sic half-bridge module for switching-loss optimization. *IEEE Trans. Ind. Appl.*, 53(4):3840–3848, July 2017.

[25] A. Endruschat, C. Novak, H. Gerstner, T. Heckel, C. Joffe, and M. Marz. A universal spice field-effect transistor model applied on sic and gan transistors. *IEEE Trans. Power Electron.*, 34(9):9131–9145, Sep. 2019.

[26] Cadence Design System, Portland, OR, USA. *Pspice A/D Reference Guide, Version 16.5*, 2011.

[27] *Wolfspeed, LTspice and PLECS Models.*

[28] M. Tapia. Use of superposition in writing state equations for networks with excess elements. *IEEE Trans. Circuit Theory*, 17(4):624–626, Nov 1970.

[29] H. Saad, S. Dennetiére, J. Mahseredjian, P. Delarue, X. Guillaud, J. Peralta, and S. Nguefeu. Modular multilevel converter models for electromagnetic transients. *IEEE Trans. Power Del.*, 29:1481–1489, June 2014.

[30] D. W. Spier, E. Prieto-Araujo, O. Gomis-Bellmunt, and J. López-Mestre. Analytic estimation of the MMC sub-module capacitor voltage ripple for balanced and unbalanced AC grid conditions. In 3^o *SiMMIER*, page 6 pp., Oct 2019.

[31] M.H.J. Bollen and L.D. Zhang. Different methods for classification of three-phase unbalanced voltage dips due to faults. *Electr. Power Syst. Res.*, 66(1):59 – 69, 2003.